ARTICLES

Relativistic XANES calculations of Pu hydrates

A. L. Ankudinov and S. D. Conradson
MST-11, Los Alamos National Laboratory, Los Alamos, New Mexico 87545

J. Mustre de Leon
Applied Physics Department, Centro de Investigaciones y Estudios Avanzados del IPN, Unidad-Mérida, Mérida, Yucatán, 97310, Mexico

J. J. Rehr
Department of Physics, University of Washington, Seattle, Washington 98195
(Received 5 November 1997)

A theoretical analysis of x-ray absorption near edge structure (XANES) at L_3 and L_1 edges for Pu hydrates with a formal oxidation state of Pu ranging from $+3$ to $+6$, using the *ab initio* multiple scattering code FEFF7, is presented. For each hydrate our calculations reproduce well the white line intensity and relative peak positions, which are the features commonly used for formal valence identification. In order to achieve such a degree of coincidence between theory and experiment, it was necessary to use a relativistic Dirac-Fock treatment of atomic densities and mixed Dirac-Fock–local-density-approximation exchange-correlation potentials, not considered in previous actinide studies. We find that most of the white line intensity at L_3 edges originates from scattering of the photoelectron, i.e., x-ray absorption fine structure. We also show that the white line shoulder peak, present in the case of plutonyl compounds (Pu^{5+} and Pu^{6+}), is due largely to constructive interference of scattering paths containing axial oxygens. Limitations of the FEFF7 code and ways to improve the quantitative agreement between XANES calculations and experimental spectra are also discussed. [S0163-1829(98)01613-0]

I. INTRODUCTION

X-ray absorption near edge structure (XANES) spectra have long been used to distinguish between different oxidation states of the absorbing atom, with applications ranging from high-temperature superconductors to catalysts.[1] Specifically, in environmental studies of radioactive materials in aqueous solutions, the valence dependence of different XANES features such as white line intensity, the edge position, or peak positions relative to the edge has permitted the determination of formal oxidation states for different actinides.[2–4] The ability of XANES spectra to determine important aspects of actinides at low concentrations in complex matrices has led to advances in the understanding of aqueous systems of nuclear waste products,[5,6] an important issue in nuclear waste disposal.[7] While XANES spectra of uranium and neptunium have been reported,[8–10], until recently there were no systematic studies performed for plutonium. XANES spectra for four different Pu hydrates with formal oxidation states of Pu ranging from $+3$ to $+6$ were recently reported in Ref. 3. In that study a correlation between the formal oxidation state of Pu and the position of the edge in XANES spectra was found. In general, it is not practical to manufacture samples with pure oxidation states in order to provide standards for identification of oxidation states in different materials. Reliable *ab initio* XANES codes could be used to produce such standards as well as to predict spectroscopic features in new systems and to understand the origin of those features starting from the local electronic and atomic structure. Reliable XANES calculations are also important for biological materials, in which usually a very limited energy range is available for extended x-ray absorption fine structure (EXAFS) analysis, and improved XANES calculations can significantly improve structural analysis in this case.

There are four major methods that are now used to calculate XANES spectra. Single-electron, multiple-scattering[11–19] (MS), and band structure[20–25] (BS) codes were more successful in reproducing XANES spectra, since many-body effects are often canceled in polarization-averaged spectra, the MS codes proved to work very well in the EXAFS region,[26] are less reliable in XANES spectra due to the lack of a self-consistent potential and the neglect of nonspherical effects. Even though modern BS methods usually include these effects and good agreement with experiment was obtained long ago for several cases,[20] agreement is less impressive in other cases, even if core-hole effects are included in calculations via a supercell.[21] Why the BS methods, which seem to be well suited for XANES calculations, do not always work is not yet clear. It may be neglect or overestimation (via supercell) of the core-hole effects and/or other approximations in the codes [such as linear dependence of phase shifts in the linearized muffin-tin orbital (LMTO) method], or that one-electron theory is inadequate for some systems. *Ab initio* molecular orbital (MO) methods[27,28] are often restricted to small clusters and a finite basis set of wave

functions, which limits the applicability of calculations to the first 40 eV. Atomic multiplet (AM) calculations[29] are very attractive since they can include some many-body effects; however, they are based on a parametrized description of an effective Hamiltonian (ligand field parameters, Hubbard model, etc.). These parameters can be estimated from *ab initio* calculations, but they are usually adjusted to fit the experiment. Similar to MO calculations, this theory is also usually restricted to the first 40 eV from the edge, since the effective Hamiltonian and the finite wave function basis set become inadequate at higher energies. This reduces the predictive power of such calculations. However, this theory provides the best interpretation of XANES peaks in terms of localized orbitals and their splittings due to the ligand field and hopping and can test many-body effective Hamiltonians by comparing to experimental XANES spectra. Thus, atomic theory has proved useful in explaining some many-body effects, such as multielectron excitations,[30] which are also observed in an x-ray magnetic circular dichroism (XMCD).[31] Thus, despite all attempts, there is no reliable predictive XANES code which whould work in all cases. This in contrast to the EXAFS region where several MS codes [FEFF,[11,32] EXCURVE,[17] and GNXAS (Ref. 33)] are now commonly used to assist in the determination of local structure.

Different methods suggest different interpretations of the white line at the L_3 edge, the most salient feature of XANES spectra in Pu hydrates. Thus, within the AM and MO picture it is interpreted as transitions to bound nd states.[34] The BS method suggests a white line interpretation as transitions to the unfilled part of the last band.[35] For example, the x-ray emission spectroscopy is therefore used to measure the width of the filled bands. These two interpretations can be combined into a single more general interpretation of the white line as a transition to unoccupied nd states. This interpretation can be used for crystals or finite clusters. Such an interpretation has been used in order to derive XMCD sum rules,[36] and significantly simplifies XMCD analysis. However, the neglect of continuum states (ϵd) that also may contribute partially to the white line intensity leads to a typical error of the order of 10% in the determination of spin and angular momentums.[22] MS calculations concentrate on calculating the one-electron Green's function instead of individual states, and suggest a MS path interpretation of peaks instead of a state interpretation. Thus MS calculations automatically include transitions to all nd and ϵd states, and they are not well suited to assign the XANES peaks as transitions to nd states. Instead, MS theory can distinguish atomic vs a scattering origin[37] of the white line. Thus, the white line may arise mainly due to the peak in atomic background known as atomic XAFS (Ref. 38) or mainly due to the positive interference of the electronic waves scattered from the neighbors, as for all EXAFS peaks. The above scattering or path interpretation of the white line is complementary to the state interpretation. The path interpretation is traditionally used in EXAFS analysis to interpret peaks in R space. The state interpretation is commonly used in XANES analysis, since it appears to have more intuitive chemical interpretation in terms of electronic states and their splittings. It does not mean, of course, that MS calculations cannot reproduce XANES peaks. MS results should be the same as BS results, if calculations are carried out to infinite order.[39] Also, if single-electron calculations (BS and MS) do not reproduce the white line, the discrepancy could be attributed to many-body effects, such as the core-hole screening and the edge singularities of Mahan.[40] In each individual case the origin of the white line may be different, so that theoretical calculations are needed to provide an interpretation.

In this paper we present calculations of XANES spectra of Pu hydrates using the *ab initio* code FEFF7,[32] which is briefly described in Sec. II. In Sec. III we compare with experimental spectra. We focus on reproducing the XANES shape for each Pu hydrate and the trends observed in the main XANES features with the change of Pu oxidation state for the L_3 and L_1 edges, and analyzing their origin. The interpretation of the white line is discussed in Sec. IV. We conclude with a summary.

II. XANES CALCULATIONS WITH FEFF7

Multiple-scattering XANES calculations are more challenging than EXAFS calculations, since the XANES approach is much more sensitive to details of the scattering potential and high-order MS paths.[8] Thus self-consistent potential and nonspherical corrections via full potential MS theory are not needed for reliable EXAFS calculations, but may be necessary for reliable XANES calculations. Also the MS path expansion may become divergent in XANES calculations due to the increase of the mean free path and backscattering amplitude. Therefore a full MS (FMS) technique should be used in these cases.[13] However, the importance of self-consistent field (SCF), nonspherical corrections and the FMS technique depends on the actual system.

Within the MS formulation, XANES calculations depend on four main ingredients: the muffin-tin scattering potential, dipole matrix elements, the scattering t matrix t_l, and the two-center matrix elements of the free propagator G_0. A review of high-order multiple-scattering theory and its applications to x-ray absorption calculations is available at the FEFF site on the worldwide web (WWW).[41] Here we will present a summary of the main developments not included in previous calculations on actinide compounds.

The construction of the muffin-tin potential is the part of the calculation which has a stronger influence on the XANES spectra than on EXAFS. FEFF7 uses the Mattheiss prescription.[42] In this approach the total electron density is approximated by overlapped free atom densities. In this work the free atom densities are calculated using a relativistic Dirac-Fock code,[43] which leads to much better estimates of the absolute edge energies. In previous actinide calculations,[8] based on FEFF6, a Dirac-Fock-Slater atomic calculation was used to obtain the free atom electronic densities. With FEFF6 edge shifts about 100 eV were needed to get edge positions right for Pu compounds, while for FEFF7 these shifts are less than 10 eV. Within the Mattheiss prescription it is possible to choose muffin-tin radii so that muffin-tin spheres just touch or overlap by 10–30 % . A more careful approach to the potential construction would include self-consistency, and use the relativistic full potential MS theory[44] to avoid the ambiguity of overlapping muffin-tin spheres and to include the nonspherically symmetric part of potential. In order to get agreement with experiment, sometimes different potential constructions have been used for different edges of the

same material.[8] However, in the present calculations, we have used the same recipe for $L1$ edge as for $L3$, making our results more trustworthy.

The FEFF7 code uses a very rough estimate of the Fermi level position. Therefore, in the present calculations, we varied the Fermi level position in order to achieve better agreement with the white line intensity. We note, however, that these shifts were small (0–2 eV) and we use the same shifts for the L_1 and L_3 edges. Such shifts do not affect our conclusions about the nature of the white line and its interpretation. Of course, for the purpose of oxidation state calibration, it is important to fix these shifts by SCF calculations.

The photoelectron self-energy enters as an energy-dependent addition to the muffin-tin potential. The real part of the self-energy alters the relative peak positions. For Pu L edges the imaginary part of the self-energy is small in the XANES region compared to the $\Gamma_{\rm ch}$. Thus the imaginary part of the self-energy was neglected in our XANES calculations. The core-hole lifetime Γ_{ch} is included at the end of the calculation by a Lorentzian convolution. This procedure is different from that used in EXAFS calculations, where one cannot neglect the imaginary part of the self-energy, since it can grow to 5–10 eV in the ''extended'' region. For the real part of the self-energy we used a partly nonolocal Dirac-Fock–local-density-approximation (LDA) self-energy model described in Refs. 41 and 45, which yielded better agreement with experimental spectra than the commonly used LDA-like Hedin-Lundqvist (HL) self-energy.[46] We note, however, that this may be due in part to the absence of self-consistency of the potential, combined with the use of Dirac-Fock atomic densities in the Mattheiss prescription. Whether this form of the self-energy leads to better agreement with experimental spectra when self-consistent potentials are used is a matter of current study.

Once the scattering potential is constructed, the rest of ingredients of multiple-scattering theory can be calculated, using various simplifying approximations to speed up calculations. As noted by Loucks,[47] the spin-orbit (SO) interaction is primarily important only in the deep core region. Thus, one must include the SO interaction in the calculation of dipole matrix elements, where the deep core region is emphasized by the initial-state core wave function. Since in these calculations we use the spinor-relativistic Dirac equation, the SO interaction is treated naturally in the calculation of dipole-matrix elements. For the same reason, the nonrelativistic expressions for matrix elements of G_0 and a j-average calculation of the scattering t matrix,[48] which neglects the SO interaction, are adequate approximations for the relativistic XANES calculations.

Details of the input parameters used in these calculation (inputs for the code FEFF7) are listed in Appendix A. Structural parameters of the local clusters of the Pu hydrates were taken from the EXAFS analysis of Pu hydrates[49] and are summarized in Appendix B. Here we only note that Pu^{3+} and Pu^{4+} have nine and eight oxygens at equal distance, respectively, while Pu^{5+} and Pu^{6+} have the plutonyl structure; i.e., they have two oxygens closer to the Pu ion above and below the equatorial plane, and four and six equidistant oxygens in this plane, respectively.

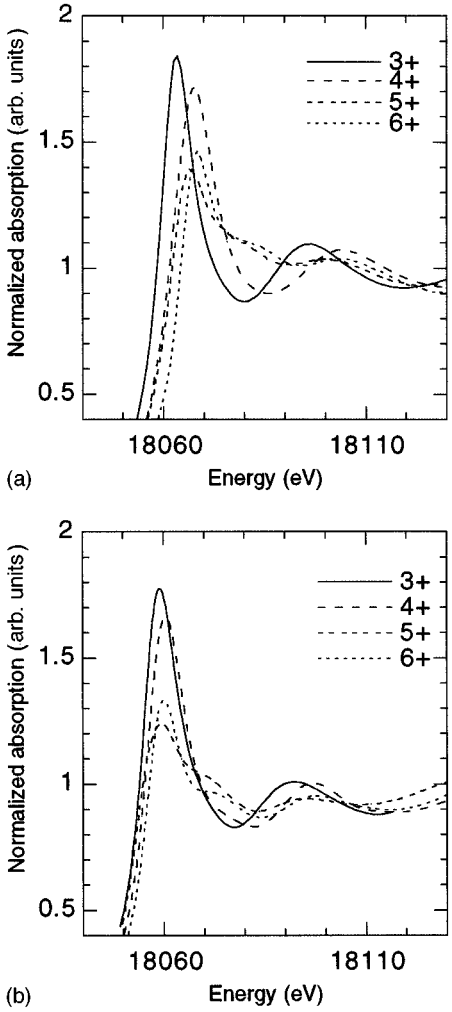

FIG. 1. L_3 edge XANES spectra of Pu hydrates: 3+ (solid line), 4+ (long dashed line), 5+ (dashed line), and 6+ (dotted line). (a) Experimental data. Note that the edge position shifts to higher energy with the increasing valence of Pu. (b) Calculations with FEFF7. Spectra are *not shifted* to match experiment. Individual shapes (white line intensity and relative peak positions) are well reproduced. Calculation of the relative edge positions compared to that in experiment needs improvement.

III. COMPARISON WITH EXPERIMENTAL SPECTRA FOR L_3 AND L_1 EDGES

Experimental L_3 edge XANES spectra for the four Pu hydrates studied are shown in Fig. 1(a). As noted in Ref. 3 there is a reduction in the white line height from Pu^{3+} to Pu^{5+} and then a small increase for Pu^{6+}. There is also a shift in the edge position. Calculated spectra, shown in Fig. 1(b), reproduce both trends, as well as higher-energy features. We note, however, that while the trend of edge position versus valence state is reproduced by the calculations, the relative edge shifts are underestimated in the calculated spectra by a few eV. This discrepancy originates in the limitations in the construction of the muffin-tin potential and errors in the calculation of the Fermi level. The crude electron-gas approximation used to calculate the Fermi level is known to yield an error of a few eV; additionally charge-transfer corrections introduced by self-consistent potentials are of the same order.[46] To illustrate the sensitivity of the XANES spectra to

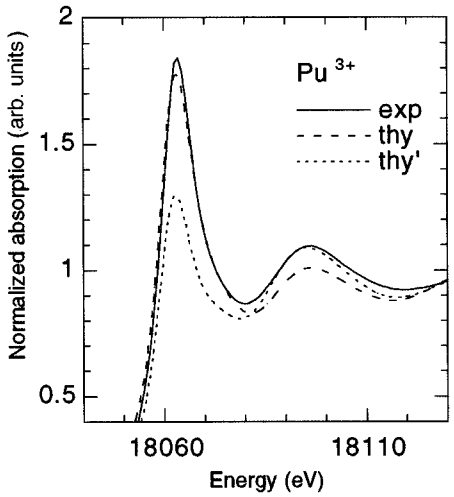

FIG. 2. L_3 edge of Pu^{3+}. The XANES spectra calculated with overlapped muffin-tin spheres (dashed line) have worse agreement with experiment (solid line) than those with a nonoverlapped muffin-tin potential (long dashed line).

details of the muffin-tin potential construction we present XANES spectra for Pu^{3+} calculated using a nonoverlapping muffin-tin potential (also shown in Fig. 2) and an overlap of 20% in the muffin-tin spheres. While in this case the use of overlapping muffin-tin spheres yields slightly worse agreement with experiment, for Pu^{5+} and Pu^{6+} it was necessary to use overlapping spheres to reproduce experimental spectra. This result is consistent with previous studies of uranyls,[2] where the authors argue that overlapping geometry should be used whenever short metal-oxygen bonds are present. We checked whether the inclusion of hydrogen atoms in the scattering cluster could yield a better prescription for the construction of the muffin-tin potential. Normally hydrogen atoms are excluded in EXAFS calculations since they do not have a significant influence due to their weak photoelectron scattering cross section. In Fig. 3 we present XANES spectra calculated including hydrogen atoms. The relative position of the edges is improved. However, the intensities of white lines are significantly reduced, yielding larger disagreements with experimental spectra. These results point out the fact that the main limitations in the XANES calculations are in our muffin-tin potential construction. Self-consistency may account for charge transfer and full potential calculations for the nonspherical corrections. It is not clear which missing part in our calculations is more important, since both may contribute to the failure of calculations which include hydrogen atoms as part of the scattering cluster.

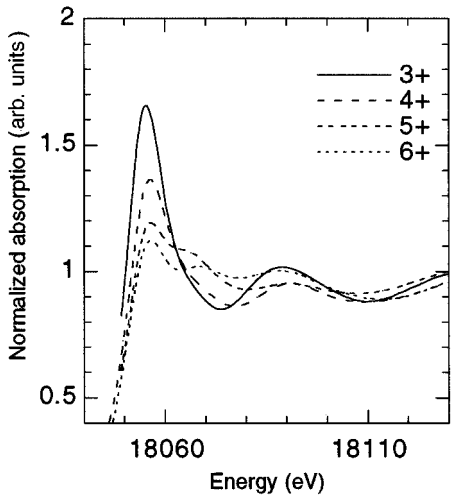

FIG. 3. Calculated L_3 edge XANES spectra of Pu hydrates. The hydrogen atoms are included in the cluster. The relative edge position is improved, but white line intensity is worse.

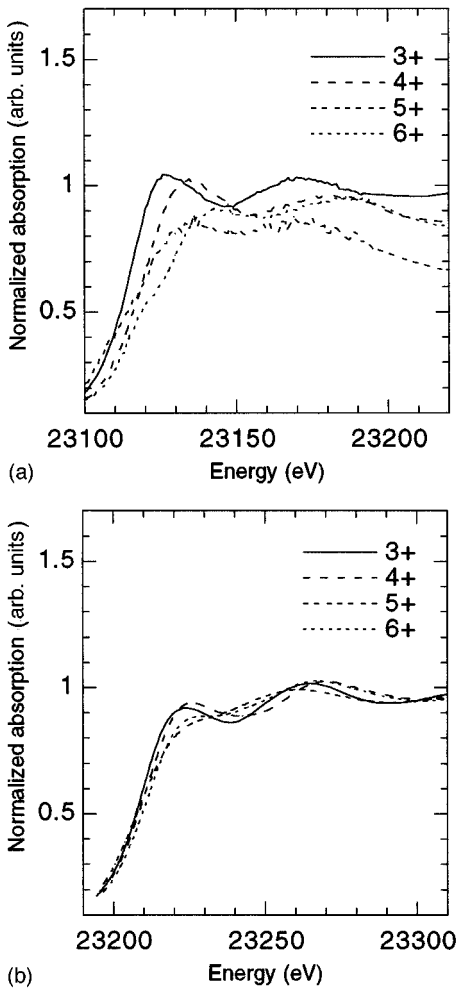

FIG. 4. L_1 edge XANES of Pu hydrates. (a) Experimental data. The first peak intensity and the slope at the edge are clearly smaller for plutonyls (Pu^{5+} and Pu^{6+}). (b) Calculations with FEFF7. The Fermi level was not adjusted in these calculations, and the same shift as for corresponding L_3 edges was used. The experimental features (reduction of first peak intensity and slope) are reproduced as well as the overall XANES shapes.

The experimental data for the L_1 edge is shown in Fig. 4(a). In this case, the free parameters which enter as part of the input in the calculation had the same values as the ones used in the corresponding L_3 edge calculations. As in the case of the L_3 edge calculations, these calculations do reproduce all individual spectral features [see Fig. 4(b)]: reduction of the first peak amplitude and slope for plutonyl compounds, and number and amplitudes of peaks. This suggests that the prescriptions used in the construction of the muffin-tin potential, and limitations in the precision of the calculation, discussed above, are independent of the edge considered.

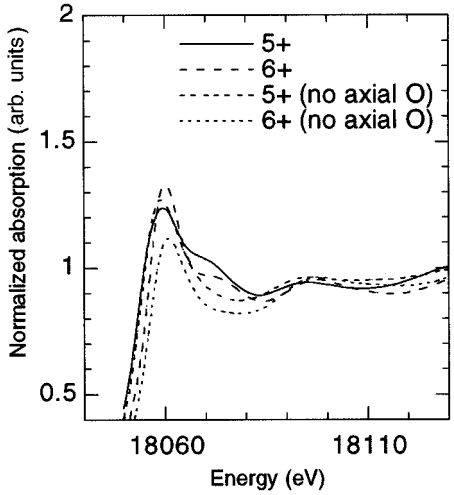

FIG. 5. Effect of axial oxygens on L_3 XANES spectra. Calculations for plutonyls with (solid line for Pu^{5+} and long dashed line for Pu^{6+}) and without axial oxygens (short dashed line for Pu^{5+} and dotted line for Pu^{6+}) show that the shoulder next to the white line is primarily due to the scattering paths containing axial oxygens.

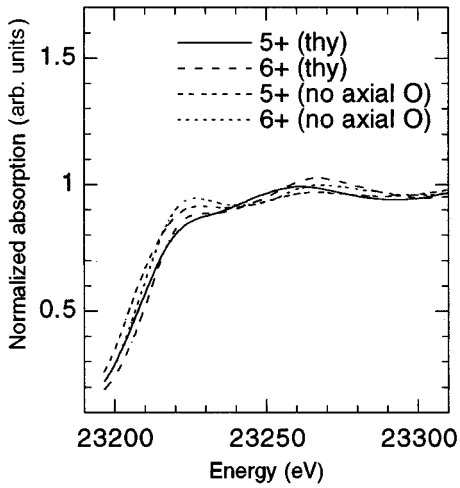

FIG. 6. Effect of axial oxygens on L_1 XANES spectra. Calculations for plutonyls with (solid line for Pu^{5+} and long dashed line for Pu^{6+}) and without axial oxygens (short dashed line for Pu^{5+} and dotted line for Pu^{6+}) show that a strong reduction of intensity and slope near the edge, noticed in experimental data, is caused by the presence of axial oxygens.

The most significant spectral feature in the L_3 XANES that distinguishes the plutonyls (Pu^{5+} and Pu^{6+}) is the appearance of the shoulder $\approx$ 10 eV above the white line and a strong reduction of the white line intensity. For uranyls it was shown by Hudson *et al.*[8] that the shoulder next to the white line is determined by the presence of axial oxygens. This hypothesis is confirmed for plutonyls (see Fig. 5). In this figure we excluded from the calculations all scattering paths which include the plutonyl oxygens. The exclusion of axial oxygens in the calculation also affects strongly the L_1 edges, as shown on Fig. 6. In this case the intensity at the edge and the slope are significantly higher in the calculations in which the axial oxygens were excluded.

We note that we were unable to reproduce even the XANES shapes for all the Pu hydrates using the code FEFF6, which has been used in similar uranyl studies to explain specific features in the spectra, e.g., the appearance of a shoulder next to the white line whenever short actinide-oxygen distances are present.[2] Thus we attribute the success of present calculations with FEFF7 in reproducing several trends in a systematic manner to the use of relativistic Dirac-Fock (DF) atomic densities and the use of partly nonlocal DF-LDA exchange-correlation potential.

IV. WHITE LINE INTEPRETATION

The white line present at the L_2 and L_3 edges arises from transitions to unoccupied d states. Within MS theory, x-ray absorption $\mu=\mu_{at}(1+\chi)$ and ℓ-projected density of states (ℓDOS) $\rho=\rho_{at}(1+\chi)$ both have smooth backgrounds and the same oscillating function χ determines the peak positions. Thus, in general the XANES peaks should correspond to peaks in the DOS except near the edge (Fermi level), where the atomic background can have a sharp peak due to the behavior of dipole matrix elements. Consequently, MS calculations can clearly distinguish whether the white line peak intensity is determined by μ_{at} and thus is mainly atomic in origin or is related to χ and the white line intensity arises as result of scattering from neighboring atoms. In Fig. 6 we present the absorption for Pu^{3+}, with the contributions arising from MS and that from an isolated embeded atom. This shows that the white line arises mostly due to the XAFS (χ), while the atomic background gives a contribution of only $\sim$30%. Thus, in the case of Pu hydrates the white line appears as a result of constructive interference of MS paths, sharing the same origin as EXAFS peaks.

The bound vs continuum state interpretation of the white line can be also checked with MS calculations. The states, constructed from localized 6d orbitals, can have energies above or below the zero potential level (vacuum level). For molecules or finite clusters, the states below zero can be interpreted as bound states, but states above zero should be interpreted as metastable states, since they will strongly mix with continuum states of the same energy. Within MS theory, to decide whether a state can be identified as a bound or a metastable state in a molecule, we need to determine the position of the zero potential level. Since the Fermi level typically lies a few eV below absolute zero and within this calculation we have uncertainties in the position of the Fermi level of the same order, it is difficult to decide whether the white line represents bound or continuum states. A more accurate estimate of the Fermi level is needed. This should be checked using a self-consistent potential construction and full potential calculations.

As noted in the Introduction, the state interpretation is impractical to be carried with MS calculations and should be done with AM, MO, or BS calculations. Since our single-electron calculations reproduce all four Pu hydrate XANES spectra, this suggests that many-body effects play a small role. Also 6d states are completely unoccupied in all four cases. Thus, if one interprets the white lines as transitions to unoccupied 6d states, the integrated intensity of the white line should be approximately the same in all four cases. In Fig. 1 one can see a strong drop in integrated intensity from Pu^{4+} to Pu^{5+}. The only reasonble way to explain this is to

interpret the shoulder for Pu^{5+} also as a transition to unoccupied $6d$ states. The increase of shoulder intensity compensates for the decrease of white line intensity. The added intensity of the white line plus the shoulder seems to be conserved for both theory and experiment.

The interpretation of the white line as transitions to unoccupied $6d$ states allows one to explain the behavior of the white line intensity from Pu^{3+} to Pu^{6+} in a simple form. If no neighboring atoms were present, all $6d$ states will have the same energy. Transitions to these states will show up in the spectrum as a Lorentzian peak with a width ≈ 10 eV (core-hole lifetime broadening). When neighbors are present, because of the nonspherical ''crystal field'' the $6d$ energy level will be split; such splitting would increase when neighbors are placed closer. Thus the white line should become broader and have a lower intensity, which is the trend observed from Pu^{3+} to Pu^{4+}. The big energy splitting of $6d$ states for Pu^{5+} and Pu^{6+} arises due to the presence of a close axial oxygen in these hydrates. The d orbital with density along this axis will have a higher energy than the d orbital with density in the equatorial plane. Thus for plutonyls (Pu^{5+} and Pu^{6+}) we associate the shoulder with metastable $6d$ states with density oriented along the plutonyl bond axis, and the white line with d states oriented in equatorial plane. The anomalous increase of the white line intensity from Pu^{5+} to Pu^{6+} can also be explained within this interpretation. The effect is similar similar to the reduction of intensity from Pu^{3+} to Pu^{4+}. In the first case the number of equatorial ligands increases from 4 to 6, and in the second case the total number of water ligands is reduced from 9 to 8. It will be interesting to see whether AM theory can confirm this interpretation of the white line. The splitting between the white line and the shoulder is about 10 eV and it seems to be too big to be explained by a ligand field. This splitting for the $3d$ level is typically only about 2 eV.[29]

However, the state interpretation does not seem to be adequate for the L_1 edge, where one can expect the behavior of $7p$ states to be similar to that of $6d$ states. Thus in Fig. 4 and Fig. 5 one does not see strong white line, which already assumes strong mixing of $7p$ and ϵp states. One also expects splitting between $7p_{x,y}$ and $7p_z$ states, which is not observed either in theory or experiment. In the case of L_1 there is no additional peak for plutonyls, which would explain the reduction of the first peak intensity, interpreted as transitions to unccupied $7p$ states. Therefore the state interpretation does not give a qualitative explanation of the spectral XANES features for L_1 edge. On the other hand, our MS calculations qualitatively reproduce all the features, and show (Fig. 7) that a reduction of the slope and first peak intensity is really connected to the structural properties: i.e., the presence of plutonyl oxygens in Pu^{5+} and Pu^{6+}. We note that for structural analysis it is essential connect observed structural properties (XAFS) to spectral features (XANES); the simulations carried with our code achieve this purpose.

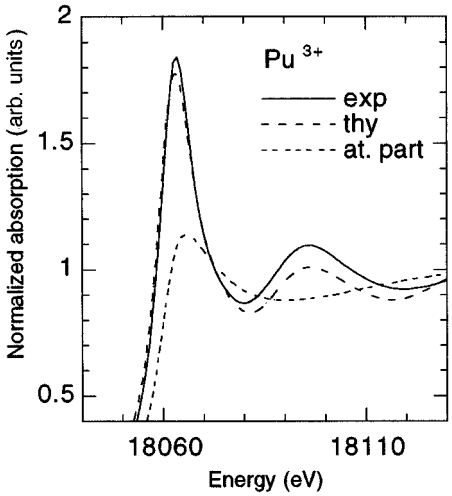

FIG. 7. Scattering origin of the white line is shown on example of the Pu^{3+} L_3 edge. The calculated embedded atom background absorption (short dashed line) has a small increase at the edge, which shows that the white line for Pu hydrates cannot have an atomic origin. Therefore the white line is a result of constructive interference of MS paths.

V. SUMMARY

XANES calculations performed with the *ab initio* code FEFF7 reproduce all the features of the individual XANES spectra for the four Pu hydrates for both L_3 and L_1 edges. Although the trend in edge position with increasing formal oxidation state is reproduced, there are quantitative discrepancies in the relative edge positions. A better potential construction is needed to reproduce the quantitative dependence. We find that the use of Dirac-Fock atomic densities and a partly nonlocal exchange-correlation potential yields better results for XANES calculations than their local-density-approximation counterparts, used in previous calculations on actinides. Overlapping muffin-tin potentials were found necessary to reproduce the XANES spectra in Pu^{5+} and Pu^{6+} for plutonyls, in agreement with studies of uranyls.[2] However, for Pu^{3+} and Pu^{4+}, the overlapping geometry yielded worse results. The two axial oxygens present in plutonyl structures (Pu^{5+} and Pu^{6+}) are shown to be responsible for the appearance of the white line shoulder in case of L_2,L_3 edges, and for the strong reduction of the slope and the first peak intensity in case of L_1 edge spectra.

Both the white line and it shoulder at the L_3 edge of Pu hydrates are best interpreted as XAFS (χ), or constructive interference of scattering paths. The contribution to white line intensity from atomic background (AXAFS) is not negligible, constituting of the order of one-third of the amplitude.

The alternative qualitative interpretation of the white line and its shoulder as transitions to unoccupied $6d$ states is complementary to the path interpretation. This interpretation can be used to qualitatively understand the behavior of their intensities with structural changes from Pu^{3+} to Pu^{6+} hydrate. However, such an interpretation cannot explain spectral features for the L_1 edge. Theoretical simulations with our code, which reproduce spectral features for both L_1 and L_3 edges, are more appropriate for the interpretation of XANES features in terms of the structural properties.

The good agreement between experiment and our calculations shows that the approximations used in the FEFF7 code are adequate for reproducing the XANES spectra even for heavy elements. Future developments of the code may even further improve XANES calculations and reduce number of

free parameters. Thus self-consistent calculations are expected to account for charge transfer and fix the Fermi level position. The use of the full potential MS theory may account for the nonspherical corrections and remove the freedom in muffin-tin geometry.

ACKNOWLEDGMENTS

The authors thank D.L. Clark, N.J. Hess, M.P. Neu, P.D. Palmer, L. Pastizzo, and C.D. Tait for the help in obtaining experimental data and useful discussions. J.M.L. acknowledges support from CONACyT-Mexico and the hospitality of the Los Alamos National Laboratory. One of us (J.J.R.) acknowledges support from the U.S. DOE under Grant No. DE-FG03-97ER45623/A000. Experimental measurements were made at SSRL, which is operated by the U.S. Department of Energy, Office of Basic Energy Sciences, Divisions of Chemical Sciences and Material Sciences.

APPENDIX A

In this appendix we list the specific input cards used in the FEFF7 input file.

(1) The XANES card should be specified. It is important to have accurate atomic positions in the cluster (ATOMS card). We used the atomic positions obtained from EXAFS analysis for these materials.

(2) Use the RPHASES (real phase shifts) card to discard the imaginary part of the self-energy. We found that the use of partially nonlocal self-energy[45] (EXCHANGE 5) worked best for the Pu hydrates.

(3) AFOLP (overlapped muffin tins) and ION cards both affect the muffin-tin potential. However, we did not use ION for any of the Pu hydrates. If AFOLP is specified, then the overlapped muffin-tin potential is constructed; otherwise, the muffin-tin spheres are just touching. We found that AFOLP give better results for Pu^{5+} and Pu^{6+}, but not for Pu^{3+} and Pu^{4+}.

(4) The use of the (CORRECTIONS vr0 vi0) card is necessary since FEFF7 makes a very crude electron-gas estimate of the Fermi level. By specifiing vr0 the Fermi level can be shifted up and down. We used vr0 = -2–0 eV and vi0 = 0 eV.

(5) The path filters should be adjusted for each particular case (CRITERIA and PCRITERIA cards). XANES calculations may require more paths than EXAFS calculations. So one has to allow more paths with path filters. One of the ways is to make all filters as small as possible for reliable XANES calculations. These path filters were set to zero, and the path list was determined by specifying RMAX 7.0 (maximum path length 14 Å). Due to the small core hole lifetime (Γ_{ch})$\geqslant$10 eV, the effective mean free path is short and the contribution from long paths is strongly suppressed.

APPENDIX B

Structural parameters of the Pu hydrates.[49]

Pu^{3+}: nine water molecules form a tricapped trigonal pyramid with an equal Pu–O distance 2.48 Å.

Pu^{4+}: eight water molecules form a cube with an equal Pu–O distance 2.39 Å.

Pu^{5+} and Pu^{6+} hydrates have the plutonyl structure: i.e., they have two short Pu–O bonds along one axis and several water molecules in the equatorial plane (perpendicular to the axis).

Pu^{5+}: short Pu–O bond is 1.84 Å, and four water molecules form a square in the equatorial plane with Pu–O distance 2.45 Å.

Pu^{6+}: short Pu–O bond is 1.74 Å, and six water molecules form a hexagon in the equatorial plane with Pu–O distance 2.45 Å.

[1] A. Bianconi, in *X-ray Absorption: Principles, Applications, Techniques of EXAFS, SEXAFS, and XANES*, edited by D. C. Konongsberger and R. Prins (John Wiley & Sons, New York, 1988), Vol. 92, p. 573.

[2] E. A. Hudson, P. G. Allen, L. J. Terminello, M. A. Denecke, and T. Reich, Phys. Rev. B **54**, 156 (1996).

[3] S. D. Conradson, I. Al Mahamid, D. L. Clark, N. J. Hess, E. A. Hudson, M. P. Neu, P. D. Palmer, W. H. Runde, and C. D. Tait, Polyhedron (to be published).

[4] D. E. Morris, P. G. Allen, J. M. Berg, C. J. Chisholm-Brause, S. D. Conradson, R. J. Donohoe, N. J. Hess, J. A. Musgrave, and C. D. Tait, Environ. Sci. Technol. **30**, 2322 (1996).

[5] P. G. Allen, J. J. Bucher, D. L. Clark, N. M. Edelstein, S. A. Eckberg, J. W. Gohdes, E. A. Hudson, N. Kaltsoyannis, W. W. Luckens, M. P. Neu, P. D. Palmer, T. Reich, D. K. Shuh, C. D. Tate, and B. D. Zwick, Inorg. Chem. **34**, 4797 (1995).

[6] P. G. Allen, D. K. Shuh, J. J. Bucher, N. M. Edelstein, T. Reich, M. A. Denecke, and H. Nitsche, Inorg. Chem. **35**, 784 (1996).

[7] K. D. Crawley, Phys. Today **50(6)**, 32 (1997).

[8] E. A. Hudson, J. J. Rehr, and J. J. Bucher, Phys. Rev. B **52**, 13 815 (1995).

[9] G. Kalkowski, G. Kaindl, W. D. Brewer, and W. Krone, Phys. Rev. B **35**, 2667 (1987).

[10] G. Kalkowski, G. Kaindl, S. Bertram, G. Schmeitser, J. Rebizant, J.C. Spirlet, and O. Vogt, Solid State Commun. **64**, 193 (1987).

[11] S. I. Zabinsky, J. J. Rehr, A. Ankudinov, R. C. Albers, and M. J. Eller, Phys. Rev. B **52**, 2995 (1995).

[12] Z. Y. Wu, T. A. Tyson, and C. R. Natoli, Physica B **208&209**, 611 (1995).

[13] P. J. Durham, J. B. Pendry, and C. H. Hodges, Comput. Phys. Commun. **25**, 193 (1982).

[14] D. D. Vvedensky, D. K. Saldin, and J. B. Pendry, Comput. Phys. Commun. **40**, 421 (1986).

[15] T. A. Tyson, K. Hodgson, C. R. Natoli, and M. Benfatto, Phys. Rev. B **46**, 5997 (1992).

[16] Z. Y. Wu, G. Ouvrard, P. Gressier, and C. R. Natoli, Phys. Rev. B **55**, 10 382 (1997).

[17] N. Binsted, S. L. Cook, J. Evans, G. N. Greaves, and R. J. Price, J. Am. Chem. Soc. **109**, 3669 (1987).

[18] N. Binsted and S. S. Hasnain, J. Synchrotron Radiat. **3**, 185 (1996).

[19] V. L. Shneerson, W. T. Tysoe, and D. K. Saldin, Phys. Rev. B **51**, 13 015 (1995).

[20] J. E. Müller and J. W. Wilkins, Phys. Rev. B **29**, 4331 (1984).
[21] M. Alouani, Phys. Rev. B **49**, 16 038 (1994).
[22] R. Wu, D. Wang, and A. J. Freeman, Phys. Rev. Lett. **71**, 3581 (1993).
[23] H. Ebert, J. Stöhr, S. S. P. Parkin, M. Samant, and A. Nilsson, Phys. Rev. B **53**, 16 067 (1996).
[24] J. E. Müller, O. Jepsen, and J. W. Wilkins, Solid State Commun. **42**, 365 (1982).
[25] R. C. Albers, A. K. McMahan, and J. E. Müller, Phys. Rev. B **31**, 3435 (1985).
[26] M. Vaarkamp, I. Dring, R. J. Oldman, E. A. Stern, and D. C. Koningsberger, Phys. Rev. B **50**, 7872 (1994).
[27] D. E. Ellis and G. L. Goodman, Int. J. Quantum Chem. **25**, 185 (1984).
[28] I. Tanaka and H. Adachi, J. Phys. D **29**, 1725 (1996).
[29] F. M. F. de Groot, J. Electron Spectrosc. Relat. Phenom. **67**, 529 (1994).
[30] E. Dartyge, A. Fontaine, Ch. Giorgetti, S. Pizzini, F. Baudelet, G. Krill, Ch. Brouder, and J.-P. Kappler, Phys. Rev. B **46**, 3155 (1992).
[31] J. Chaboy, A. Marcelli, and T. A. Tyson, Phys. Rev. B **49**, 11 652 (1994).
[32] A. L. Ankudinov and J. J. Rehr, Phys. Rev. B **56**, R1712 (1997).
[33] A. Filipponi, A. Di Cicco, and C. R. Natoli, Phys. Rev. B **52**, 15 122 (1995).
[34] B. Rupp, Phys. Rev. B **49**, 12 278 (1994).
[35] See, for example, L. V. Azaroff and D. M. Pease, in *X-ray Spectroscopy*, edited by L. V. Azaroff (McGraw-Hill, New York, 1974); in *Soft X-ray Band Spectra and the Electronic Structure of Metals*, edited by D. J. Fabian (Academic, New York, 1968).
[36] B. T. Thole, P. Carra, F. Sette, and G. van der Laan, Phys. Rev. Lett. **68**, 1943 (1992); P. Carra, B. T. Thole, M. Altarelli, and X. Wang, *ibid.* **70**, 694 (1993); A. Ankudinov and J. J. Rehr, Phys. Rev. B **51**, 1282 (1995).
[37] B. W. Holland, J. B. Pendry, R. F. Pettifer, and J. Bordas, J. Phys. C **11**, 633 (1978).
[38] J. J. Rehr, S. I. Zabinsky, A. Ankudinov, and R. C. Albers, Physica B **208&209**, 23 (1995).
[39] W. L. Schaich, Phys. Rev. B **8**, 4028 (1973).
[40] G. D. Mahan, in *Solid State Physics*, edited by H. Ehrenreich *et al.* (Academic Press, New York, 1974), Vol. 29, p. 75.
[41] A. L. Ankoudinov, Ph.D. thesis, University of Washington, 1996.
[42] L. Mattheiss, Phys. Rev. **133**, A1399 (1964).
[43] A. L. Ankudinov, S. I. Zabinsky, and J. J. Rehr, Comput. Phys. Commun. **98**, 359 (1996).
[44] X. Wang, X.-G. Zhang, W. H. Butler, B. N. Harmon, and G. M. Stocks, in *Application of Multiple Scattering Theory to Materials Science*, edited by W. H. Butler, P. H. Dederichs, and A. Gonis, MRS Symposia Proceedings No. 253 (Materials Research Society, Pittsburgh, 1992), p. 211.
[45] A. L. Ankudinov and J. J. Rehr, J. Phys. (France) IV Colloq. **7**, C2-121 (1997).
[46] J. Mustre de Leon, J. J. Rehr, S. I. Zabinsky, and R. C. Albers-,Phys. Rev. B **44**, 4146 (1991).
[47] T. L. Loucks, *Augmented Plane Wave Method* (Benjamin, New York, 1967).
[48] D. D. Koelling and B. N. Harmon, J. Phys. C **10**, 3107 (1977).
[49] S. D. Conradson, D. L. Clark, M. P. Neu, C. D. Tait, W. Runde, and P. D. Palmer (unpublished).